PCCP

Radiation-Induced Reaction Kinetics of Zn^{2+} with e_S^- and $Cl_2^{\bullet-}$ in Molten LiCl-KCl Eutectic at 400-600°C

Journal:	*Physical Chemistry Chemical Physics*
Manuscript ID	CP-ART-03-2022-001194.R1
Article Type:	Paper
Date Submitted by the Author:	27-Apr-2022
Complete List of Authors:	Iwamatsu, Kazuhiro; Brookhaven National Laboratory Department of Chemistry Horne, Gregory; Idaho National Laboratory, Center for Radiation Chemistry Research Gakhar, Ruchi; Idaho National Laboratory Research Library, Nuclear Science and Technology Halstenberg, Phillip; University of Tennessee Knoxville, Department of Chemistry Layne, Bobby; Brookhaven National Laboratory, Department of Chemistry Pimblott, Simon M.; Idaho National Laboratory, Nuclear Science & Technology Wishart, James; Brookhaven National Laboratory, Department of Chemisty

ARTICLE

Radiation-Induced Reaction Kinetics of Zn^{2+} with e_S^- and $Cl_2^{\bullet-}$ in Molten LiCl-KCl Eutectic at 400-600 °C

Received 00th March 2022,
Accepted 00th April 2022

DOI: 10.1039/x0xx00000x

Kazuhiro Iwamatsu,[a]* Gregory P. Horne,[b]* Ruchi Gakhar,[b] Phillip Halstenberg,[c] Bobby Layne,[a] Simon M. Pimblott,[b] and James F. Wishart[a]

Molten chloride salts are currently under consideration as combined coolant and liquid fuel for next-generation molten salt nuclear reactors. Unlike complimentary light-water reactor technologies, the radiation science underpinning molten salts is in its infancy, and thus requires a fundamental mechanistic investigation to elucidate the radiation-driven chemistry within molten salt reactors. Here we present an electron pulse radiolysis kinetics study into the behaviour of the primary radiolytic species generated in molten chloride systems, i.e., the solvated electron (e_S^-) and di-chlorine radical anion ($Cl_2^{\bullet-}$). We examine the reaction of e_s^- with Zn^{2+} from 400-600 °C (E_a = 30.31 ± 0.09 kJ mol^{-1}), and the kinetics and decay mechanisms of $Cl_2^{\bullet-}$ in molten lithium chloride-potassium chloride (LiCl-KCl) eutectic. In the absence of Zn^{2+}, the lifetime of e_s^- was found to be dictated by residual impurities in ostensibly "pure" salts, and thus the observed decay is dependent on sample history rather than being an intrinsic property of the salt. The decay of $Cl_2^{\bullet-}$ is complex, owing to the competition of $Cl_2^{\bullet-}$ disproportionation with several other chemical pathways, one of which involves reduction by radiolytically-produced Zn^+ species. Overall, the reported findings demonstrate the richness and complexity of chemistry involving the interactions of ionizing radiation with molten salts.

Introduction

Interest in the chemistry of molten salts in radiation environments is in resurgence due to the potential of molten salt reactors (MSRs) to revolutionize the nuclear energy landscape.[1,2] Both fluoride and chloride salt systems have been proposed as reactor coolant and fuel matrix candidates. However, the radiation science underpinning molten salts is in its infancy compared to water radiolysis, which is critically important for managing water-cooled reactor technologies. [3-5,] In parallel to safety and corrosion concerns associated with the formation of molecular hydrogen (H_2) and hydrogen peroxide (H_2O_2) from water radiolysis, the formation of volatile, corrosive species (e.g., chlorine and fluorine gas) and changes in metal ion speciation from molten salt radiolysis are worrisome to MSR development. This knowledge gap in the radiation chemistry of molten salts is in part due to the extreme environments necessary to perform such investigations (i.e., high temperatures coupled with corrosive media and intense ionizing radiation fields), and because early MSR studies concluded that radiation-induced chemical changes were absent in the molten state.[6] Subsequently, and to the contrary, several studies reported radiation-induced formation of oxidizing and reducing transients in a variety of alkali metal halide molten salt systems.[7-14] These studies have shown that the absorption of ionizing radiation by molten halide salt systems (represented as M^+X^-) initiates production of an energetic excess electron (e^-) and corresponding 'hole' (electron vacancy) that localizes on the halide component (X^-) to produce a halide radical ($X^\bullet$). As in water, the initial energetic e^- passes through states of partial or pre-solvation prior to complete solvation (e_S^-, absorbing in the visible and near-IR), while $X^\bullet$ rapidly forms an anion-radical dimer with other halide anions ($X_2^{\bullet-}$, predominantly absorbing in the UV):[11,15,16]

$$M^+X^- \rightsquigarrow M^+ + X^\bullet + e^-, \quad (1)$$

$$e^- \rightarrow e_{pre}^- \rightarrow e_s^-, \quad (2)$$

$$X^\bullet + X^- \rightarrow X_2^{\bullet-}. \quad (3)$$

The identification and optical characterization of these transient species in molten salt systems is fundamentally significant, as they are analogous to the highly-reactive hydrated electron (e_{aq}^-) and hydroxyl radical ($^\bullet$OH) produced by water radiolysis, and thus are expected to participate in similar chemical reactivity that may negatively influence MSR performance and durability.[3]

Consequently, understanding the reactivity of e_s^- and $X_2^{\bullet-}$ in molten salt solutions is necessary to determine the effects of radiation on the physical and chemical properties of molten salt matrices for reactor applications. Further, radiation-driven chemistry may also lead to the degradation of reactor materials, e.g., the metal alloys used for MSR vessels. Elucidating the

[a] Brookhaven National Laboratory, Upton, New York, 11973, USA.
[b] Idaho National Laboratory, 1955 N. Freemont Ave., Idaho Falls, 83415, USA.
[c] Oak Ridge National Laboratory Oak Ridge, TN 37830, USA.
* Corresponding authors: iwamatsu@bnl.gov and gregory.horne@inl.gov

† Electronic Supplementary Information (ESI) available: **Salt purification apparatus schematics, high-temperature-controlled Van de Graaff cuvette holder, temperature dependent reaction kinetics at 700 nm, time dependent spectra at 400 °C, and 240 nm transient absorption kinetics at 400 °C**. See DOI: 10.1039/**x0xx00000x**

fundamental properties of radiation-induced transients has historically been achieved by scavenger studies utilizing electron pulse radiolysis techniques, whereby solutes are introduced to react with said transients, confirming their identification, and establishing their chemical reactivity.[3, 17] Pikaev and coworkers performed the most extensive investigation to date into the reactions of e_S^- with scavengers and of $X_2^{\bullet-}$ with radiolysis products in molten salt systems.[9,11] They observed the absorption spectra of e_S^- and $X_2^{\bullet-}$ in several neat molten salt systems, their eutectics, and other mixtures, obtaining apparent second-order rate coefficients (k) for e_S^- scavenging by divalent barium (Ba^{2+}), strontium (Sr^{2+}), calcium (Ca^{2+}), cadmium (Cd^{2+}), and zinc (Zn^{2+}) ions, and by monovalent tellurium (Tl^+) and silver (Ag^+) ions in molten sodium chloride (NaCl), potassium chloride (KCl), and potassium bromide (KBr) systems using an indirect method based on initial absorbance ratios as a function of scavenger concentration. However, due to the relatively long (2.3 μs) width of the electron pulses from their accelerator, overlap with the observed electron decay kinetics resulted in reported rate coefficient uncertainties of ~30%. Pikaev and coworkers also examined the second-order decay kinetics of $X_2^{\bullet-}$ reacting, according to their interpretation, with the reduced parent salt dimer metal cation (M_2^+) or with monovalent calcium (Ca^+), zinc (Zn^+), or cadmium (Cd^+) ions formed by e_S^- scavenging by the corresponding divalent metal ions.

More recently, Sawamura and coworkers performed nanosecond electron pulse radiolysis experiments on molten lithium chloride-potassium chloride (LiCl-KCl), lithium bromide-potassium bromide (LiBr-KBr), lithium fluoride-potassium fluoride (LiF-KF), and lithium fluoride-sodium fluoride-potassium fluoride (LiF-NaF-KF) systems.[12,13,14] In each salt system, they observed the absorption band of e_S^-, with peak absorbances between 500 and 800 nm depending on salt mixture composition and temperature, which decayed via first-order kinetics with lifetimes on the order of hundreds of nanoseconds. In each case, the addition of 50 mM Cd^{2+} caused the e_S^- absorption band to disappear, and the appearance of an additional absorption with a peak around 330 nm that indicated the formation of Cd^+. Reaction rate coefficients for the scavenging of e_S^- by Cd^{2+} were not determined for any of these salt systems. However, in the chloride and bromide cases, rate coefficients and activation energies (E_a) for the observed second-order decay of $X_2^{\bullet-}$ (measured at 340 and 360 nm, respectively) were reported.

The work described above demonstrates that there is rich chemistry involving the interactions of ionizing radiation with molten salts, which will be especially important for the design, development, and deployment of MSRs. However, very large areas of molten salt radiation-induced chemical kinetics and reaction mechanisms remain undetermined. For example, in the studies cited above, the mechanism of e_S^- decay in the absence of scavengers was generally attributed to reaction with the metal cation of the bulk salt to form an alkali metal atom (M^0) or dimer metal cation (M_2^+) without any specific proof.[9] This interpretation would seem to be unlikely because alkali metals dissociate into cations and e_S^- when they are added to molten alkali salts in low concentrations (on a par with pulse radiolysis conditions).[18-20] At higher concentrations, electron pairing (bipolaron formation) occurs.[20] Since it is very difficult to purify salts and avoid contamination from oxygen, moisture, or other materials, it is much more likely that similar residual impurities are responsible for decay of e_S^- in ostensibly "pure" salts,[12,13] and, consequently, the observed decay would be dependent on sample history rather than being an intrinsic property of the salt, with the result being that scavenging rate coefficients that are referenced in competition to these processes might not be reliable.[9,11]

Here we present a focused effort towards the development of more quantitative and detailed insights into the radiation-driven chemistry of molten salt systems by examining the reaction of e_S^- with Zn^{2+} and the kinetics and mechanism of di-chlorine radical anion ($Cl_2^{\bullet-}$) decay in molten LiCl-KCl eutectic at 400-600 °C.

Experimental

Chemicals. Acetone (≥99.5% purity, ACS reagent), isopropanol (≥99.5% purity, ACS reagent), lithium chloride-potassium chloride eutectic (LiCl-KCl, anhydrous beads, 99.99% trace metal basis), nitric acid (HNO_3, ≥99.999% trace metals basis), potassium chloride (KCl, ≥99.999%, Suprapur®), potassium thiocyanate (KSCN, ≥99.0% ACS Reagent Grade), and zinc chloride (99.99% purity, trace metals basis) were sourced from Sigma-Aldrich and used without further purification. Zinc chloride ($ZnCl_2$, anhydrous, free-flowing, Redi-Dri™, reagent grade, ≥98% purity) was purified and prepared at as described below, and different concentrations of $ZnCl_2$ in LiCl-KCl were prepared by mixing the purified salt with the eutectic of the mixed alkali metal salts. Argon gas (Ar, >99.998%) nitrogen (N_2, >99.998%) and nitrous oxide (N_2O, UHP) were purchased from Airgas USA, LLC.

Sample Preparation. Commercial $ZnCl_2$ was purified by distillation.[21,22] The distillation apparatus was a three-chamber fused silica tube with each chamber separated by a quartz slide insert fused to the walls of the tube, shown in *Electronic Supplementary Information* (ESI) **Figs. S1** and **S2**. The salt was loaded into the chamber furthest from the opening via a funnel inside a N_2-atmosphere glovebox. Once loaded into the column, the end was sealed with a compression fitting connected to a Teflon stopcock. The column was placed in a three-inch tube furnace and a vacuum line was connected to the column through the fitting. The valve was opened, and the column evacuated until the pressure reached ~1×10^{-3} Torr. After evacuation, the tube furnace was programmed to reach a setpoint of 800 °C at a ramp rate of 10 °C min^{-1} from room temperature. The column remained at the setpoint under dynamic vacuum until approximately 80% of the original volume of salt added to the column had sublimed and re-condensed in the chamber closest to the opening of the column. After enough of the salt had collected in the condensation chamber, the valve was closed while still under vacuum and the column transferred into the glovebox. Once in the glovebox, the

column was refilled with a N_2-atmosphere and the compression fitting removed. The column was then inverted, and the distillate recovered from the collection chamber. The distilled salt was then transferred to a glass jar with a Teflon-lined lid for shipment.

The preparation of salt mixtures involved mixing $ZnCl_2$ with LiCl-KCl in a glassy carbon crucible (GAT6, 64 mL Sigradur tapered crucible) in an Ar-atmosphere glovebox. The glassy carbon crucibles were rinsed with acetone and isopropanol, dried in a vacuum oven at 150 °C for 3 hours and then dried inside an Ar-atmosphere glovebox at 600 °C overnight prior to use, to remove any residue. The desired amount of $ZnCl_2$ and LiCl-KCl eutectic salts were weighed using a Mettler Toledo microbalance. The contents were left to melt at 450 °C for 3 hours, to ensure complete homogeneity. The salt systems were then allowed to solidify and cool, prior to removal from the crucible and being broken into small chunks for loading into quartz radiolysis cells.

Inductively Coupled Plasma Mass Spectrometry Analysis. Quantification of Zn^{2+} in salt mixtures was performed by elemental analysis at INL using a Perkin Elmer 350D Inductively Coupled Plasma Mass Spectrometer (ICP-MS). Instrument parameters were held constant at 8 mL min^{-1} Ar plasma flow, 0.7 mL min^{-1} Ar nebulizer gas flow, 0.2 mL min^{-1} Ar auxiliary gas flow, 1600 watts radio frequency (RF) power, and introduction pump at 1 mL min^{-1} flow to the spray chamber. Zinc standards, for calibration and quality control, were prepared at concentrations between 5 and 1000 ng mL^{-1}. Approximately 0.5 g of each solid salt sample was dissolved in 10 mL total volume of 7% trace metal grade HNO_3 and appropriately diluted for quantitative analysis. The relative percent precision of the ICP-MS determinations for all analytes was better than 2%.

Time-Resolved Pulse Radiolysis Experiments. Molten salt reaction kinetics were investigated using the Brookhaven National Laboratory (BNL) Laser-Electron Accelerator Facility (LEAF) and Van de Graaff electron pulse radiolysis/transient absorption systems.[23,24] Samples of pure $ZnCl_2$ (m.p. 293 °C) and LiCl-KCl eutectic (58 mol% LiCl, 42 mol% KCl, m.p. 357 °C) containing $ZnCl_2$, were received sealed in custom 5 × 5 mm Spectrosil® Quartz fluorescence cuvettes (Starna, Inc.), with stems terminating in Teflon valves. Prior to irradiation, the Ar-atmosphere inside the sample cuvettes was evacuated to avoid cell rupture by gas expansion upon heating. Samples were then loaded into bespoke, high-temperature-controlled cuvette holders, and heated to above their respective melting points (400 °C for neat $ZnCl_2$ and 400-600 °C for LiCl-KCl) and allowed to thermally equilibrate for at least 10 minutes prior to study. Sample temperatures were monitored using a thermocouple installed in the sample holder's heating block, located less than 1 cm between the sample cuvette and heater. Temperature variations were determined to be less than ± 1.0°C during each experiment. Measurements at a given temperature were made over a period of 5-10 minutes, and were found to be self-consistent, indicating that there was no significant temperature variation between measurements over this time frame. For LEAF experiments, the design and fabrication of the high-temperature-controlled cuvette holder has been previously discussed.[25] For Van de Graaff experiments, a new high-temperature-controlled cuvette holder was developed and is discussed in ESI **Fig. S3**.

Radiation-induced reactions were initiated by either 30 ps- or 7 ns-long, 8.7 MeV electron pulses from the BNL LEAF accelerator,[23] and by 2 us-long, 2.0 MeV electron pulses from the Van de Graaff accelerator. For LEAF experiments, pulse widths were determined by the choice of the laser system used to illuminate the accelerator's magnesium photocathode. For the 30 ps-long electron pulse, a 3 ps pulse from a tripled (266 nm) Ti-Sapphire laser was used, while a 7 ns electron pulse from a quadrupled (266 nm) Nd:YAG laser was used for the 7 ns-long pulse. Transient kinetics were followed at selected wavelengths (300-1000 nm) using either an FND-100QH (EG&G Optoelectronics) or S5973-01 (Hamamatsu) silicon photodiode detector and recorded with either a LeCroy WaveRunner HRO 66Zi (600 MHz, 12 bit) or LeCroy 640Zi (4 GHz, 8 bit) oscilloscope, depending on the time resolution required. Interference filters (10 nm bandpass for 800 nm or less, 25 nm bandpass above 800 nm, Edmund Optics) were used for wavelength selection of the analyzing light. For Van de Graaff experiments, the electron pulse width was controlled by a pulsed electrical potential to the thermionic cathode. A monochromator (Gemini 180, Horiba) and appropriate long-pass filters (200, 250, 280, 385, 475 and 630 nm) were used for wavelength selection of the analyzing light. Optical signals were recorded using a photomultiplier tube (9659QB, EMI Electronic) and LeCroy HDO 4034 oscilloscope (350 MHz, 12 bit). Data acquisition at both accelerators is controlled by LabVIEW software (National Instruments) and collected transient absorption data was stored and analyzed using Igor Pro (Wavemetrics).

Electron pulse dosimetry was determined at ambient temperature using N_2O-saturated, aqueous 10 mM KSCN solutions measured at λ_{max} = 470 nm ($G\varepsilon$ = 5.08 × 10^4 m^2 J^{-1}, where G is the radiolytic yield in mol J^{-1}, and ε is the molar extinction coefficient in M^{-1} cm^{-1})[26] and corrected for the relative electron density difference between the dosimetry solution and the investigated molten salt systems. Second-order rate coefficients (k) were either derived from linear fits to pseudo first-order (k') e_S^- decays rates as a function of solute (i.e., Zn^{2+}) concentration, or by taking the fitted slope of the reciprocal absorbance plot at 340 nm for $Cl_2^{\bullet-}$ decay. Transient absorbances were also used to calculate the product $G\varepsilon$, by using the known absorbed dose and optical path length. Quoted errors are a combination of measurement precision and sample concentration errors.

Absorption Spectra Kinetic Analysis. The acquired data matrix of time resolved absorption spectra and kinetics were comprised of multiple species and absorption components. Data deconvolution was achieved by a combination of singular value decomposition (SVD) and multivariate curve resolution alternating least squares (MCR-ALS) methods using *Spectro-Kinetic Analysis* (SK-Ana).[27] Positive constraints for spectra and kinetics were imposed for the analysis.

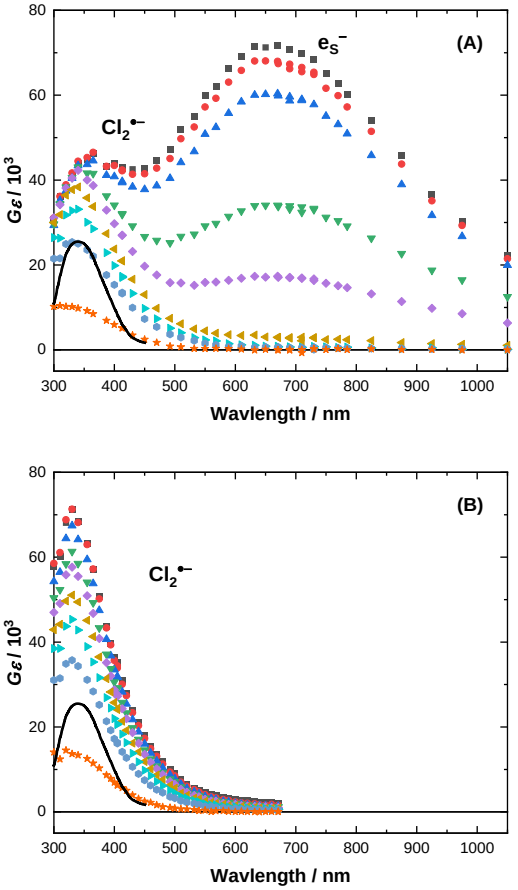

Fig. 1. Transient absorption spectra at selected times: 5 ns (■), 10 ns (●), 20 ns (▲), 100 ns (▼), 200 ns (◆), 500 ns (◀), 1 µs (▶), 2 µs (⬢) and 10 µs (★) at 400 °C: **(A)** neat LiCl-KCl and **(B)** 142 mM $ZnCl_2$ in LiCl-KCl. The transient molten salt spectra are compared with the spectrum for $Cl_2^{\bullet-}$ in water derived from reference 28, indicated with a solid black line.

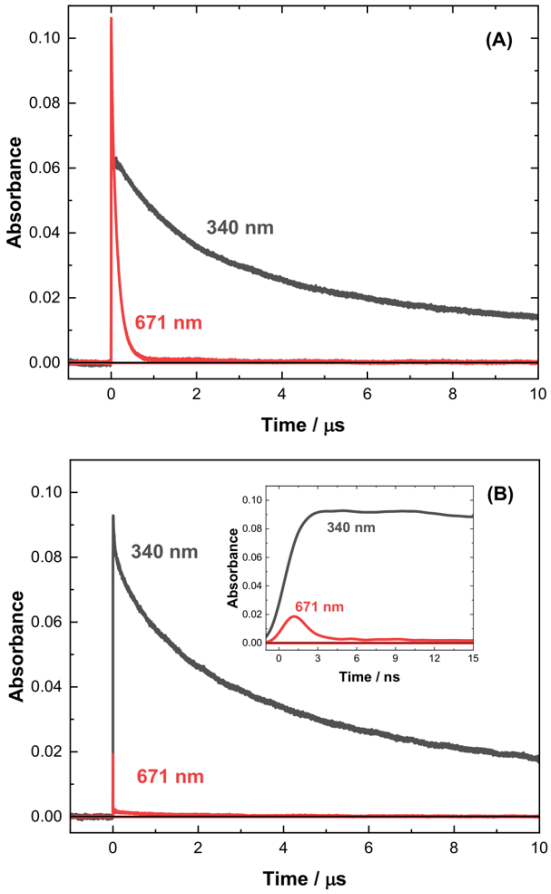

Fig. 2. Decay kinetics for e_S^- (●) and $Cl_2^{\bullet-}$ (■) measured at 671 and 340 nm, respectively: **(A)** neat LiCl-KCl and **(B)** 142 mM $ZnCl_2$ in LiCl-KCl at 400 °C. *Inset*: Early-time kinetics.

Results and Discussion

Molten LiCl-KCl Radiolysis. The transient absorption spectra and decay kinetics at selected wavelengths from the pulse radiolysis of molten LiCl-KCl at 400 °C are shown in **Figs. 1 (A)** and **2 (A)**, respectively. Two major transient species can be distinguished from the spectra shown in **Fig. 1 (A)**, one in the visible to near-IR region and the second in the UV region. In agreement with Hagiwara *et al.*,[12] the first transient exhibits a broad absorption spectrum in the visible to near IR wavelength region with an absorption maximum (λ_{max}) at 660 nm that is attributed to e_S^-. This transient reducing species is formed within the rise time of the signal and exhibits a first-order decay with a lifetime of 145 ns, as shown in **Fig. 2 (A)**. Hagiwara *et al.*[12] observed a longer lifetime of 250 ns in the same salt composition, also at 400 °C. As stated in the introduction, we believe that the observed e_S^- lifetime is determined by residual reactive impurities rather than being an intrinsic property of the LiCl-KCl salt system. The manufacturer's trace metal analysis certificate for this batch (batch # 0000054157, source # 0000040181) of LiCl-KCl eutectic lists impurities as follows (in ppm): Na 26.9, Ca 4.3, Zn 3.2, Rb 3.0, Mg 2.9, Sr 2.6, and others less than 1. As these impurity abundances are of the order of µM, and some have previously been identified as electron scavengers in molten salt systems,[11] our observed e_S^- lifetime is consistent with scavenging by impurities. Scavenging by protons (H^+), produced from residual moisture that might be introduced in handling, is also a strong possibility.

The second spectroscopically-resolved transient shown in **Fig. 1 (A)** exhibits a narrower absorption spectrum in the UV region. At 5 ns after the electron pulse, this band is visible as a shoulder peak on the broad e_S^- spectrum. Once e_S^- has fully decayed (~500 ns), a band peaking at 340 nm is observed clearly; this band has been attributed previously to $Cl_2^{\bullet-}$.[7-13] Support for this assignment is also given by comparison of this band with the known absorption spectrum of $Cl_2^{\bullet-}$ in aqueous solution,[28] overlaid to scale with a solid black line in **Fig. 1 (A)** and **(B)**. The molten salt and aqueous peak absorption wavelengths (λ_{max}) are close, although we note that the absorption profile of $Cl_2^{\bullet-}$ in molten LiCl-KCl is broader, particularly on the red side. As is evident from **Fig. 2 (A)**, $Cl_2^{\bullet-}$ decays at a much slower rate (~10^5 s^{-1}) than e_S^-, and by a process that is predominantly second-order (*vide infra*). Interestingly, following the decay of $Cl_2^{\bullet-}$, a residual transient is observed in the UV region at ≥ 10 µs in **Fig. 1 (A)** and **(B)**.

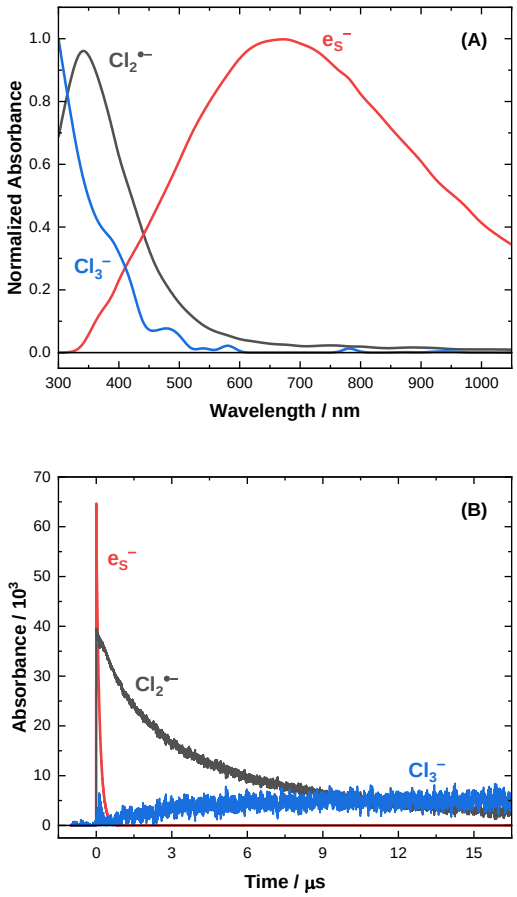

Fig. 3. Normalized spectra from SK-Ana deconvolution **(A)** and complimentary kinetic contributions at each peak wavelength **(B)** for neat LiCl-KCl at 400 °C.

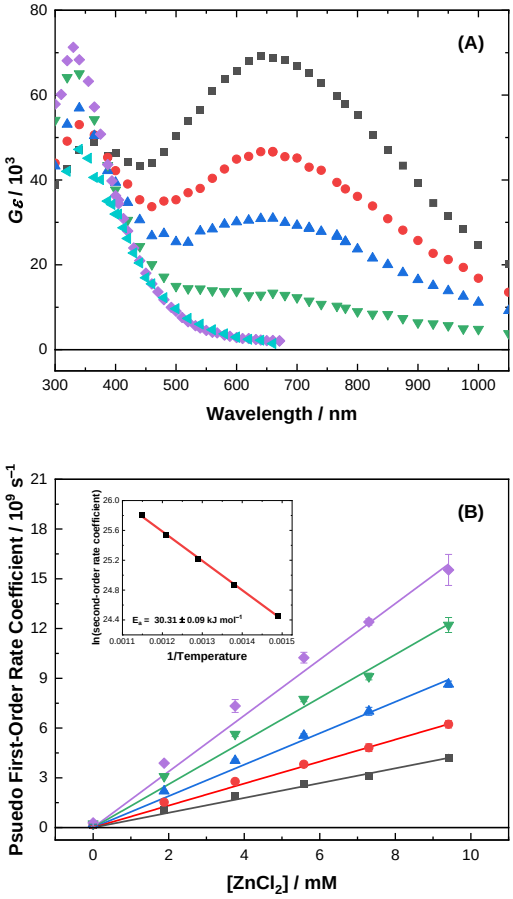

Fig. 4. (A) Transient absorption spectra at 5 ns after pulse as a function of $ZnCl_2$ concentration: 0 (■), 1.88 (●), 3.76 (▲), 9.41 (▼), and 142 mM (◆) $ZnCl_2$ in LiCl-KCl, and neat $ZnCl_2$ (◀) at 400 °C. **(B)** Observed pseudo first-order rate coefficients measured at 700 nm as a function of $ZnCl_2$ concentration and temperature: 400 (■), 450 (●), 500 (▲), 550 (▼), and 600 °C (◆). Solid lines are linear fits to data, for which the gradient corresponds to the second-order rate coefficient at a given temperature. *Inset:* Arrhenius plot, E_a = 30.31 ± 0.09 kJ mol^{-1}.

Deconvolution of these time-resolved absorption spectra and associated kinetics was achieved by *SK-Ana* analysis.[27] The results for neat LiCl-KCl at 400 °C are shown in **Fig. 3 (A)** and **(B)**, respectively. The spectra for e_S^- and $Cl_2^{\bullet-}$ were obtained from early time scale data (~1 μs) using multiple data matrices to reduce the effect of products and ambiguity on the shape of the spectra. The two spectra were clearly separated, and were used as constraints for longer time (~20 μs) SK-Ana calculations to derive the three components shown **Fig. 3**. The deconvoluted kinetics for e_S^- and $Cl_2^{\bullet-}$ in **Fig. 3 (B)** are in good agreement with our experimentally resolved data shown in **Fig. 2 (A)**. The aforementioned UV region residual at ≥ 10 μs, i.e., the third component in **Fig. 3.**, is attributed to the trichloride anion (Cl_3^-) generated from the disproportionation of $Cl_2^{\bullet-}$:

$$Cl_2^{\bullet-} + Cl_2^{\bullet-} \rightarrow Cl_3^- + Cl^-, \quad (4)$$

as its yield increases as $Cl_2^{\bullet-}$ decreases. Furthermore, the λ_{max} for Cl_3^- in aqueous solution has been reported at 220 nm with a large molar extinction coefficient, ε = 10400 ± 200 M^{-1} cm^{-1},[29] which agrees with the *SK-Ana* spectra prediction and our assignment. Although we still observe a residual transient in the UV region in **Fig. 1 (B)**, the profile and associated kinetics of this species are different and attributed here to the low oxidation state Zn^+ cations, for which a more detailed discussion is presented below.

Effect of Zn^{2+} on e_S^-. The transient absorption spectra at selected times after pulse radiolysis of 142 mM Zn^{2+} in molten LiCl-KCl are shown in **Fig. 1 (B)**. Comparison of **Fig. 1 (A)** and **1 (B)** clearly shows that the presence of Zn^{2+} suppresses the e_S^- absorption band in the visible to near-IR and increases the intensity of the $Cl_2^{\bullet-}$ UV absorption band, **Fig. 1 (B)**. These spectral observations are also evident in the corresponding kinetic growth and decay traces shown in **Fig. 2 (A)** and **(B)**.

The absorption intensity of e_S^- is progressively reduced with increasing Zn^{2+} concentration, as shown in **Fig. 4 (A)**. These observations are indicative of e_S^- scavenging by Zn^{2+}, in agreement with observations reported by Pikaev *et al.*:[9,11]

$$Zn^{2+} + e_s^- \rightarrow Zn^+, \quad (5)$$

and consistent with previous measurements for the reaction of Zn^{2+} with the e_{aq}^- from water radiolysis:[30-35]

$$Zn^{2+} + e_{aq}^- \rightarrow Zn^+ \quad k_6 = 1.5 \times 10^9\ M^{-1}\ s^{-1}.[29] \quad (6)$$

Here, analysis of the transient decay of e_S^- at 700 nm as a function of Zn^{2+} concentration (0-9.41 mM) and temperature (400-600 °C) in molten LiCl-KCl afforded second-order rate

coefficients of k_5 = (4.2-16.1) × 10^{10} M^{-1} s^{-1}. The pseudo-first order kinetics as a function of Zn^{2+} concentration are shown in **Fig. 4 (B)**, and the individual kinetics per temperature in ESI **Fig. S3**. Pikaev *et al.* reported rate coefficients for **Eq. (5)** in other molten chloride salt systems using microsecond electron pulse radiolysis: k_5 = 1.7 × 10^9 M^{-1} s^{-1} in NaCl at 850 °C, and 2.8 × 10^9 M^{-1} s^{-1} in KCl at 800 °C.[11] However, these values are essentially best-guess estimates, as they are based on observed e_S^- yields at the edge of a 2.3 μs-long electron pulse, and thus do not account for shorter time-scale processes, the importance of which are clearly shown in **Fig. 2 (A)** and **(B)**, and ESI **Fig. S3**. The coefficients presented here are obtained directly from well-resolved decay curves that include nanosecond time-scale kinetics. The corresponding Arrhenius plot for **Eq. (5)** is shown in the inset of **Fig. 4 (B)**, yielding an E_a = 30.31 ± 0.09 kJ mol^{-1}.

Electron scavenging by Zn^{2+} is not limited to only the reaction with e_S^- as described above, it may be further deconvoluted based on the electron's level of solvation. As indicated in Eq. **(2)**, the excess electron (e^-) goes through stages of partial or pre-solvation before becoming completely solvated. The thermal precursor (e_{pre}^-) to e_S^- may also be subject to scavenging by Zn^{2+}:

$$Zn^{2+} + e_{pre}^- \rightarrow Zn^+. \quad (7)$$

Partitioning between these electron scavenging reactions, **Eqs. (5)** and **(7)**, can only be indirectly determined with our current experimental time resolution, since precursor scavenging processes are typically gated by the timescale of solvation,[40] which we expect to be on the picosecond timescale. However, evidence for precursor scavenging by Zn^{2+} was obtained by the classical method[36-39] of extrapolating the e_S^- decay curves (400 °C data in ESI **Fig. S4**) back to time zero. The initial yield of e_S^-, estimated from extrapolation, decreases with increasing Zn^{2+} concentration, which is indicative of precursor scavenging. Additionally, the corresponding C_{37} value—the concentration of scavenger needed to decrease the yield of e_S^- to 37% ($1/\varepsilon$)—is estimated to be 77 ± 10 mM Zn^{2+} in molten LiCl-KCl at 400 °C. C_{37} values below 100 mM are indicative of high reactivity towards e_{pre}^-.[36-40]

Effect of Zn^{2+} on $Cl_2^{\bullet-}$. As previously highlighted, the absorption intensity of the $Cl_2^{\bullet-}$ UV absorption band increases in the presence of Zn^{2+}, relative to neat molten LiCl-KCl, as shown in **Fig. 2 (A)** and **(B)**. The absorption intensity ($G\varepsilon$) of $Cl_2^{\bullet-}$ at 340 nm, where there is no overlap at any timescale between the respective absorption bands of $Cl_2^{\bullet-}$ and e_S^-, increases by ~45% (47000 to 65000 m^2 J^{-1}) in going from 0 to 9.41 mM Zn^{2+} and settles at ~55% (68000 m^2 J^{-1}) for 142 mM Zn^{2+}, owing to either complete inhibition of electron-mediated processes and/or overlapped spectra with reduced Zn^{2+} species.

In the absence of Zn^{2+}, excess electrons (e_i^- = e^-, e_{pre}^-, and e_S^-) can either recombine with $Cl^\bullet$ (through geminate and non-geminate recombination processes), reduce surrounding metal cations (M^{n+}), and/or react with $Cl_2^{\bullet-}$:[41]

$$Cl^\bullet + e_i^- \rightarrow Cl^-, \quad (8)$$

$$M^{n+} + e_i^- \rightarrow M^{\bullet(n-1)+}, \quad (9)$$

$$Cl_2^{\bullet-} + e_i^- \rightarrow 2Cl^-. \quad (10)$$

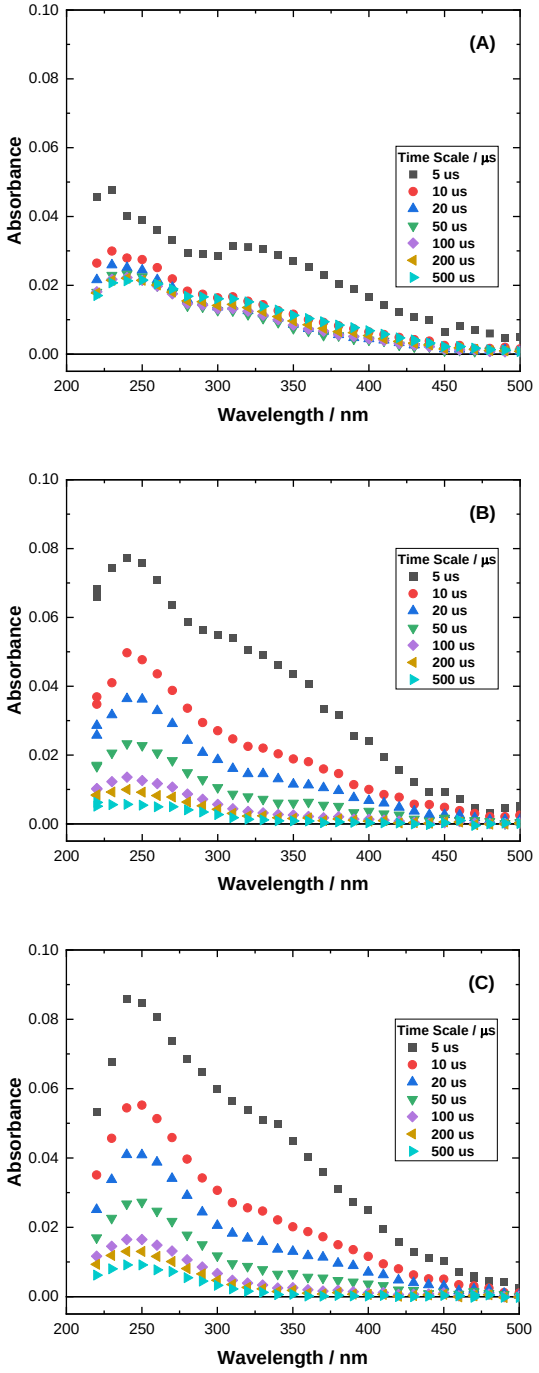

Fig. 5. Absorption spectra at longer time scales for neat LiCl-KCl **(A)** and 10 **(B)** and 50 **(C)** mM $ZnCl_2$ in LiCl-KCl at 400 °C.

Although Li^+ and K^+ reduction is possible in molten LiCl-KCl, the rate of monovalent cation reduction by e_i^- would appear to be slow, which may explain the relatively long decay of e_S^- in neat LiCl-KCl, **Fig. 2 (A)**. Further, reduction of Li^+ and K^+ affords neutral metal atoms (M^0) which can be expected to undergo rapid dissociation based on the measured e_S^- lifetime:

$$M^0 \rightarrow M^+ + e^-. \quad (11)$$

This interpretation is consistent with our findings and those of Pikaev and coworkers,[11] and is supported by the absence of an e_s^- signal in neat molten $ZnCl_2$, **ESI Fig. S5**. Consequently, in the presence of Zn^{2+}, the recombination processes **Eqs. (8)** and **(10)** are progressively disfavoured with increasing Zn^{2+} concentration as the effectiveness of **Eq. (9)** increases, affording the larger observed yield of $Cl_2^{\bullet-}$ in **Fig. 2 (B)**.

Further, the observed absorption at 240 nm in the absence of Zn^{2+} in **Fig. 5 (A)** is attributed to Cl_3^-. The absorption of Cl_3^- initially (~2 μs onwards, **Fig. 5 (A)**) decreases due to its dissociation into Cl^- and Cl_2:

$$Cl_3^- \rightleftharpoons Cl^- + Cl_2. \quad (12)$$

However, after ~100 μs, the equilibrium of **Eq. (12)** is established, resulting in the observed plateau in the Cl_3^- absorption **Fig. 5 (A)**. In the presence of Zn^{2+}, **Fig. 5 (B)** and **(C)**, the absorption at 240 nm is made up of contributions from both Cl_3^- and Zn^+. Although there is no spectral data for Zn^+ in molten salts, Zn^+ has been reported to exhibit a peak at λ_{max} = 300 nm in aqueous media.[42] Further, there is also evidence for relatively long-lived metal dimers (M_2^{n+}) below 300 nm.[42,43] In this work, the kinetic lifetime of the transient with the absorption maximum at 240 nm, **Fig. 5 (B)** and **(C)**, decreases with increasing Zn^{2+} concentration (e.g., ~9.5 μs for 10 mM Zn^{2+} and ~4.0 μs for 50 mM Zn^{2+}, estimated from **ESI Fig. S6**), suggesting a reaction between zinc dimer ions (Zn_2^{n+}) and/or other zinc species (Zn^{2+}, Zn^+, and/or Zn_2^{n+}).

The observed decay of $Cl_2^{\bullet-}$ as a function of Zn^{2+} concentration at 340 nm is shown in **Fig. 6 (A)**, for which the candidate decay mechanisms are $Cl_2^{\bullet-}$ disproportionation (**Eq. (4)**) and reduction by reaction with Zn^+ (**Eq. (13)**) produced by **Eq. (9)**, where $M^{n+} = Zn^{2+}$:[11]

$$Cl_2^{\bullet-} + Zn^+ \rightarrow 2Cl^- + Zn^{2+}, \quad (13)$$

Both **Eqs. (4)** and **(13)** imply that we should observe kinetics that are second order with respect to radiolytic dose; **Eq. (4)** being the model of A + A, and **Eq. (13)** being the model of A + B where [A] ≅ [B]. If either case applies, a reciprocal plot (of 1/absorbance *vs.* time) should produce a straight line with a slope of $2k/\varepsilon l$ or $k/\varepsilon l$, respectively. The inset graph in **Fig. 6 (A)** shows that is indeed the case for 3.76-9.41 mM $ZnCl_2$ in LiCl-KCl, but not for neat LiCl-KCl or neat $ZnCl_2$.

The fact that the reciprocal plots for the $ZnCl_2$ solutions in LiCl-KCl are linear implies that one of the two reactions in **Eqs. (4)** and **(13)** is faster and therefore dominant. For reasons that will be explained below, we believe that **Eq. (13)** prevails. For one thing, the asymptotic slope of the black trace for neat LiCl-KCl at long time in the inset of **Fig. 6 (A)** is substantially less than when millimolar levels of $ZnCl_2$ are present. Metal cation mediated $Cl_2^{\bullet-}$ reduction has been reported for several metal cations in various molten salt solutions.[11,44] For example, Zn^+ has been shown to reduce the di-bromine radical anion ($Br_2^{\bullet-}$) with a rate coefficient of 7.0×10^{10} M^{-1} s^{-1} at 800 °C.[11]

As seen in **Fig. 6 (A)** the reciprocal plot for neat $ZnCl_2$ is curved at short timescales (< 1 μs), while for neat LiCl-KCl the curvature covers essentially the entire time window. Curvature in the reciprocal plots for the neat salts indicates that an additional $Cl_2^{\bullet-}$ loss mechanism is significant and required to

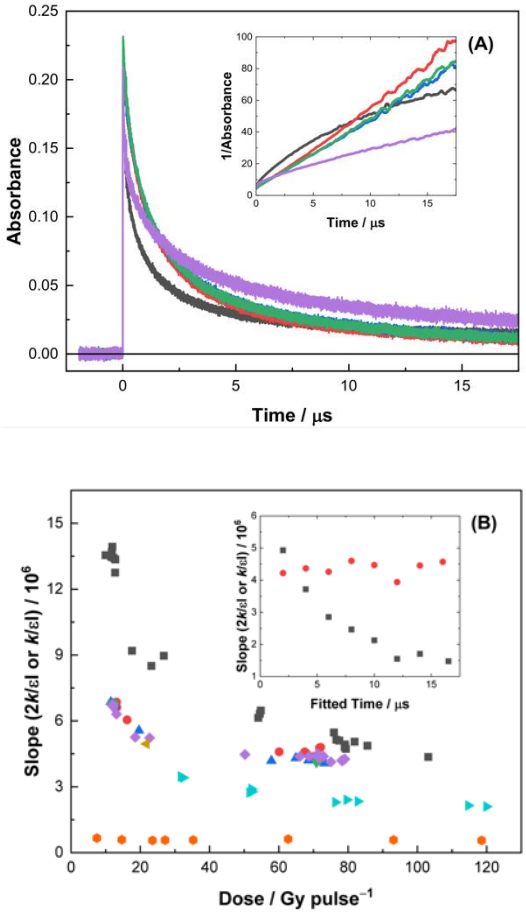

Fig. 6. (A) Transient absorption kinetics at 340 nm as a function of $ZnCl_2$ concentration: 0 (black), 3.76 (red), 7.30 (blue), 9.41 (green) mM $ZnCl_2$ in LiCl-KCl, and neat $ZnCl_2$ (purple) at 400 °C (Dose 70-77 Gy/pulse). *Inset:* Reciprocal plot (1/absorbance), for which the fitted time scales are 1-10 μs, except for neat LiCl-KCl, which was from 1-5 μs. **(B)** Reciprocal plot slopes ($2k/\varepsilon l$ for bimolecular reactions, and k/ε; for mixed reactions) estimated from fitting at 1-5 μs as a function of dose for $Cl_2^{\bullet-}$ in: 0 (■), 3.76 (●), 5.88 (▲), 7.30 (▼) 9.41 (◆), and 142 mM (◀) $ZnCl_2$ in LiCl-KCl, and neat $ZnCl_2$ (▶) at 400 °C. The decay of $(SCN)_2^{\bullet-}$ (⬢) from the decay of aqueous 10 mM KSCN is also included. *Inset:* Difference in slop values ($2k/\varepsilon l$ or k/ε) at different fitting time scales for neat LiCl-KCl (■) and 9.41 mM $ZnCl_2$ in LiCl-KCl (●).

describe the system. As in the case of the electron-scavenging impurities discussed above, the presence of inadvertent $Cl_2^{\bullet-}$ scavengers (S or S^-) due to impurities in even highly purified salts is practically inevitable. Two mechanisms might apply: direct reaction of the impurity S with $Cl_2^{\bullet-}$, **Eq. (14)**, and electron capture by S followed by the reaction of S^- with $Cl_2^{\bullet-}$ **Eqs. (15)** and **(16)**, where **Eq. (15a)** applies to LiCl-KCl and **Eq. (15b)** applies to neat $ZnCl_2$.

$$Cl_2^{\bullet-} + S \rightarrow 2Cl^- + S^+, \quad (14)$$

$$S + e_s^- \rightarrow S^-, \quad (15a)$$

$$S + Zn^+ \rightarrow S^- + Zn^{2+}, \quad (15b)$$

$$Cl_2^{\bullet-} + S^- \rightarrow 2Cl^- + S. \quad (16)$$

In the case of **Eq. (14)**, S would be some sort of impurity that can be directly oxidized by $Cl_2^{\bullet-}$, and the expected kinetic form of such a reaction in the range of the radiolytic doses used here would be pseudo-first order, or mixed-order at higher doses and low [S]. The observed kinetic traces for the neat molten salts do

not seem to comport with that form. We feel it is more likely that the additional loss mechanism operates by **Eqs. (15)** and **(16)**, particularly since we attribute **Eq. (15a)** to be the principal decay mechanism for e_s^- in LiCl-KCl under our conditions. In this case, S could be H^+ or trace metal ions. **Eqs. (15a** and **15b)** limit the yield of S^- to the lesser of [S] and [e_s^-] or [Zn^+], so the kinetic form of **Eq. (16)** corresponds to the second-order model of A + B where [A] ≥ [B].

To unambiguously quantify the reactions in **Eqs. (4)** and **(13)** it is necessary to isolate them from the effects of **Eq. (16)**, which adds an obscuring faster component to the observed $Cl_2^{\bullet-}$ decay. The fact that **Eqs. (15a** and **15b)** limit the yield of S^- allows us to do that by increasing the radiolytic dose to overwhelm the effect of the scavenger. **Fig. 6 (B)** shows the effects of increasing radiolytic dose on the slopes of 1/absorbance data fitted between 1-5 μs.

Analysis of the reciprocal plot slopes in **Fig. 6 (B)** clearly shows the effects of dose. A large dose dependence is observed for neat LiCl-KCl at 400 °C, the reciprocal slopes for which decrease with increasing dose from ~1.4×10^7 to ~4.1×10^6 s^{-1}, as shown in **Fig. 6 (B)**. This decrease agrees with the premise that at lower doses in neat LiCl-KCl, both **Eqs. (4) and (16)** are responsible for the observed $Cl_2^{\bullet-}$ decay, while **Eq. (4)** gradually predominates with increasing dose, due to the greater abundance of $Cl_2^{\bullet-}$ formed per pulse. Thus, for our operating conditions, doses above 70 Gy/pulse permit us to focus on **Eq. (4)** in neat LiCl-KCl.

The Zn^{2+}-containing salt systems exhibit little to no dose dependence above 60 Gy/pulse, with plateau slope values of ~4.5×10^6 s^{-1} for 3.76-9.41 mM $ZnCl_2$ in LiCl-KCl at 400 °C, and ~2.0×10^6 s^{-1} for neat $ZnCl_2$ at 400 °C. Additionally, there is no [Zn^{2+}]-dependence of the slope values for millimolar $ZnCl_2$ concentrations in LiCl-KCl at 400 °C. This observation indicates that **Eq. (16)** is rendered ineffective because **Eq. (9)** (where M^{n+} = Zn^{2+}) outcompetes **Eq. (15a)** in the investigated $ZnCl_2$ concentration regime, and the effect of **Eq. (15b)**, if it applies, is minimized by overwhelming [S] with the larger dose. Thus, the observed slope plateau corresponds to the rate coefficient of **Eq. 13**. For lower doses (< 60 Gy $pulse^{-1}$) the effects of impurities do contribute to higher fitted slopes especially for the $ZnCl_2$ solutions in LiCl-KCl.

For comparison, the 1/absorbance slope behavior of the decay kinetics of $(SCN)_2^{\bullet-}$ in aqueous KSCN solution as a function of dose is also shown in **Fig. 6 (B)**. It is understood to undergo simple bimolecular decay via disproportionation as in **Eq. (4)**.[26] Consequently, no dependence of the observed slope with dose is observed.

The slope values presented in **Fig. 6 (B)** *Inset* are fitted over 1 μs windows at different time delays as depicted on the x-axis. Those for neat LiCl-KCl and 9.41 mM $ZnCl_2$ used higher doses (>75 Gy $pulse^{-1}$). Under these irradiation conditions, the slope decreased for neat LiCl-KCl, reaching a plateau at ~1.5×10^6 s^{-1}, whereas there was no slope change as a function of time scale in the presence of 9.41 mM Zn^{2+}. The slopes of the reciprocal plots in **Fig. 6 (B)** *Inset* are equal to 2k/εl and k/εl for neat LiCl-KCl and 9.41 mM $ZnCl_2$, respectively. The apparent rate coefficient for $Cl_2^{\bullet-}$ decay in neat LiCl-KCl was reported by

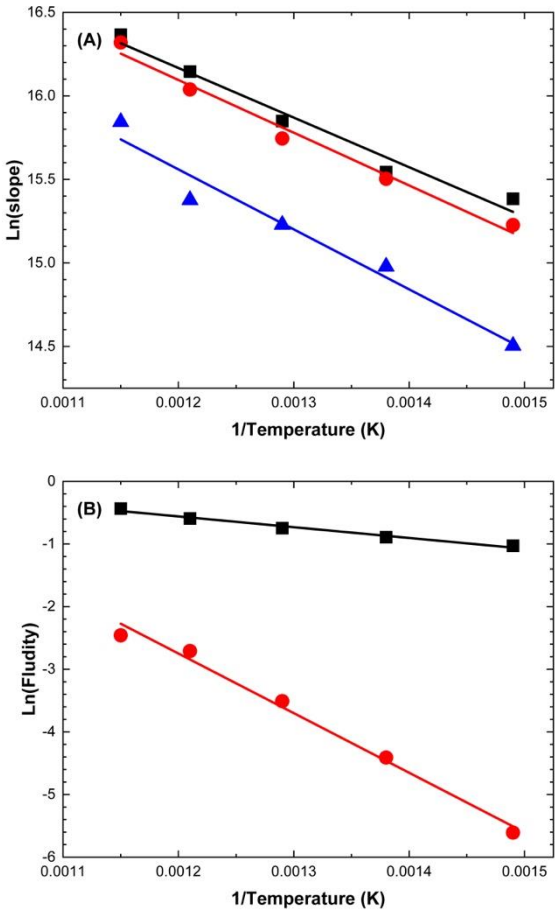

Fig. 7. (A) Arrhenius plot for $Cl_2^{\bullet-}$ decay reactions **Eq. (9)** for neat LiCl-KCl (■) and **Eq. (13)** for 9.41 mM (●) $ZnCl_2$ in LiCl-KCl and neat $ZnCl_2$ (▲) at 400 °C. **(B)** Arrhenius plot for the fluidities of neat LiCl-KCl (■) and $ZnCl_2$ (●) at 400 °C.

Hagiwara and coworkers as $k/\varepsilon l$ = 3.0×10^6 s^{-1} and attributed solely to disproportionation.[12] Their dose was 50-85 Gy per pulse, which is in the same region as that used here. Although they did not differentiate between potential $Cl_2^{\bullet-}$ decay reactions, nor report an optical path length, their apparent decay rate is consistent with our estimated value of 1.5×10^6 s^{-1}.

Rate coefficients for $Cl_2^{\bullet-}$ decay in aqueous solution have been previously reported in the range of k/ε = 2.7-9.5 × 10^5 M^{-1} s^{-1},[30-34] where $\varepsilon(Cl_2^{\bullet-}{}_{(aq)})$ was 8800 M^{-1} cm^{-1}.[28] These values are lower than those reported in molten salt systems, however, they were measured at temperatures significantly lower than the 400 °C used here. Although there are no reported values for $\varepsilon(Cl_2^{\bullet-})$ in molten LiCl-KCl salt systems, it is expected to be around 8000 M^{-1} cm^{-1}. Makarov and coworkers reported that the variation in ε with salt system formulation corresponds to the spectral width.[10] Therefore, if we employ the same ε = 8000 M^{-1} cm^{-1} to estimate the rate coefficients for **Eqs. (4)** and **(13)**, we get (2.2 ± 2.0) x 10^9 and (2.0 ± 0.2) x 10^{10} M^{-1} s^{-1}, respectively, for the system of 0-9.41 mM Zn^{2+} in LiCl-KCl at 400 °C. From these values, in conjunction with the remaining 450-600 °C data shown in **Fig. 7 (A)**, we calculate an activation energy for **Eq. (4)**, the disproportionation of $Cl_2^{\bullet-}$, of E_a = 26 ± 2 kJ mol^{-1} in LiCl-KCl, which is in good agreement with E_a = 24 kJ mol^{-1} obtained by Hagiwara and coworkers,[12] and E_a = 30 ± 3 kJ mol^{-1} for $Cl_2^{\bullet-}$

disproportionation in neat $ZnCl_2$. In the case of 9.41 mM Zn^{2+} in LiCl-KCl, the activation energy for **Eq. (13)**, the reaction of $Cl_2^{\bullet-}$ with Zn^+, $E_a = 25 \pm 3$ kJ mol^{-1}.

For comparison with the reaction activation enthalpies, the activation energies of viscous flow in the neat molten salts were calculated as shown in **Fig. 7 (B)**. $E_a = 14 \pm 2$ and 79 ± 5 kJ mol^{-1} were obtained for neat LiCl-KCl and neat $ZnCl_2$, respectively, compared to 26 and 30 kJ mol^{-1} for **Eq. (4)**. Comparison of the activation energies in LiCl-KCl (14 kJ mol^{-1} for flow or diffusion *vs.* 26 kJ mol^{-1} for **Eq. (4)**) indicates that the disproportionation of $Cl_2^{\bullet-}$ is an activated process, i.e., not diffusion-controlled. Even more remarkable is the fact that the activation energy for disproportionation in neat $ZnCl_2$ is 30 kJ mol^{-1} while that for viscous flow is 79 kJ mol^{-1}, which is consistent with its glassy nature and much higher viscosity, e.g., ~4.0 cP for neat LiCl-KCl at 400 °C, and ~360 cP for neat $ZnCl_2$ at 400 °C.[45,46] The rate coefficient we obtained for **Eq. (13)** in LiCl-KCl (2.0×10^{10} M^{-1} s^{-1}) is only 2.27× higher than the one obtained for neat $ZnCl_2$ ($(8.8 \pm 0.2) \times 10^9$ M^{-1} s^{-1}), although the viscosity is 90× lower. This implies that $Cl_2^{\bullet-}$ is diffusing more easily (and presumably faster) than the constituent ions of the molten salt. It is therefore reasonable to suggest that $Cl_2^{\bullet-}$ diffusion operates by a Grotthuss-type mechanism involving the exchange of chloride anions:

$$(Cl\text{-}Cl)^{\bullet-} + Cl^- \rightarrow Cl^- + (Cl\text{-}Cl)^{\bullet-} \quad (17)$$

Similar mechanisms have been employed to explain the transport properties of triiodide ions in iodide-based ionic liquids used in photoelectrochemical solar cells.[47,48] This provocative result requires further experimental and theoretical investigation, but if it is substantiated it has profound implications for understanding the mobility and reactivity of charge-deficient ("hole") species in halide molten salts.

Conclusions

Irradiation of molten LiCl-KCl systems yields two important observable radiolytic transients, e_S^- and $Cl_2^{\bullet-}$. In the presence of Zn^{2+}, e_S^- is rapidly scavenged at rates of $(4.2 \pm 0.1) - (16.1 \pm 0.6) \times 10^{10}$ M^{-1} s^{-1} for 400-600 °C ($E_a = 30.31 \pm 0.09$ kJ mol^{-1}), a value significantly faster than previously reported, owing to greater time-resolution afforded by picosecond electron pulse radiolysis detection. Evidence for pre-solvated electron scavenging by Zn^{2+} was observed in the kinetic data, with $C_{37} = 77 \pm 10$ mM. Consumption of e_S^- by Zn^{2+} promotes greater $Cl_2^{\bullet-}$ yields through suppression of two charge recombination processes: $Cl^\bullet + e_S^- \rightarrow Cl^-$ and $Cl_2^{\bullet-} + e_S^- \rightarrow 2Cl^-$.

Rate coefficients and activation energies for the disproportionation of $Cl_2^{\bullet-}$ and its cross-reaction with radiolytically-produced Zn^+ ($Zn^+ + Cl_2^{\bullet-} \rightarrow Zn^{2+} + 2Cl^-$) were obtained, after accounting for interference by side reactions with adventitious scavengers, by using a wide range of radiolytic doses. In LiCl-KCl at 400 °C, the cross-reaction of $Cl_2^{\bullet-}$ with Zn^+ was nine times faster than disproportionation. This is a key point because the cross-reaction is effectively a charge recombination that leads to no net radiolytic products, while disproportionation produces relatively stable Cl_3^- in equilibrium with volatile Cl_2 (+ Cl^-), possibly leading to accumulation of permanent salt radiolysis products. Long-term, stable management of MSR fuel salt depends on the dominance of charge recombination over product accumulation, and this study is just one step in establishing the knowledge base required to manage salt radiolysis issues.

Comparison of the kinetics and activation energies for $Cl_2^{\bullet-}$ reactions measured in highly fluid molten LiCl-KCl eutectic and viscous, glassy molten $ZnCl_2$ revealed that there were only small differences in the rate coefficients and activation energies measured in the two media despite their vast differences in viscosity and its temperature dependence. This evidence points towards the existence of a Grotthuss mechanism of chloride ion exchange for the diffusion of $Cl_2^{\bullet-}$, which implies a mobility significantly higher than the constituent ions of the salt. Such a mechanism for providing rapid mobility of electron-deficient halide species has positive implications for the promotion of charge recombination over permanent radiolytic product accumulation, and it deserves detailed experimental and theoretical study.

Conflicts of interest

There are no conflicts to declare.

Acknowledgements

This work was supported as part of the Molten Salts in Extreme Environments Energy Frontier Research Center, funded by the U.S. Department of Energy (US-DOE), Office of Science, Basic Energy Sciences, at BNL, INL and ORNL under contracts DE-SC0012704, DE-AC07-05ID14517, and DE-AC05-00OR22725, respectively. The Laser Electron Accelerator Facility of the BNL Accelerator Center for Energy Research is supported by the US-DOE Office of Basic Energy Sciences, Division of Chemical Sciences, Geosciences, and Biosciences under contract DE-SC0012704.

Notes and references

(1) J. Serp, M. Allibert, O. Benes, S. Delpech, O. Feynberg, V. Ghetta, D. Heur, D. Holcomb, V. Ignatiev, J.L. Kloosterman, L. Luzzi, E. Merle-Lucotte, J. Uhhr, R. Yoshioka, and D. Zhimin, *Prog. Nucl. Energy*, 2014, **77**, 308.

(2) C. Forsberg, *Nucl. Tech.*, 2020, **206 (11)**, 1659.

(3) B.C. Garrett, D.A. Dixon, D.M. Camaioni, D.M. Chipman, M.A. Johnson, C.D. Jonah, G.A. Kimmel, J.H. Miller, T.N. Rescigno, P.J. Rossky, S.S. Xantheas, S.D. Colson, A.H. Laufer, D. Ray, P.F. Barbara, D.M. Bartels, K.H. Becker, K.H. Bowen, S.E. Bradforth, I. Carmichael, J.V. Coe, L.R. Corrales, J.P. Cowin, M. Dupuis, K.B. Eisenthal, J.A. Franz, M.S. Gutowski, K.D. Jordan, B.D. Kay, J.A. LaVerne, S.V. Lymar, T.E. Madey, C.W. McCurdy,

D. Meisel, S. Mukamel, A.R. Nilsson, T.M. Orlando, N.G. Petrik, S.M. Pimblott, J.R. Rustad, G.K. Schenter, S.J. Singer, A. Tokmakoff, L.-S. Wang, and T.S. Zwier, *Chem. Rev.*, 2005, **105 (1)**, 355.

(4) A.J. Elliot and D.M. Bartels, The Reaction Set, Rate Constants and G-Values for the Simulation of the Radiolysis of Light Water Over the Range 20° to 350° C Based on Information Available in 2008. AECL Nuclear Platform Research and Development – Report 153-127160-450- 001. 2009.

(5) G.V. Buxton, C.L. Greenstock, W.P. Helman, and A.B. Ross, *J. Phys. Chem. Ref. Data*, 1988, **17 (2)**, 513.

(6) W.R. Grimes, ORNL-TM-1853, 1967.

(7) I.E. Makarov, T.N. Zhukova, and A.K. Pikaev, *Radiat. Effects*, 1974, **22**, 71.

(8) I.E. Makarov, T.N. Zhukova, and A.K. Pikaev, *Dokl. Akad. Nauk SSSR*, 1975, **225 (5)**, 1103.

(9) A.K. Pikaev, B.G. Ershov, and I.E., Makarov, *J. Phys. Chem.*, 1975, **79**, 3025.

(10) I.E. Makarov, T.N. Zhukova, A.K. Pikaev, and V.I. Spistyn, *Bull. Acad. Sci. USSR, Div. Chem. Sci. (Engl. Transl.),* 1982, **31(4)**, 662.

(11) A. K. Pikaev, I. E. Makarov, and T. N. Zhukova, *Radiat. Phys. Chem.*, 1982, **19**, 377.

(12) H. Hagiwara, S. Sawamura, T. Sumiyoshi, and M. Katayama, *Radiat. Phys. Chem.*, 1987, **30**, 141.

(13) S. Sawamura, J. L. Gebicki, J. Mayer, and J. Kroh, *Radiat. Phys. Chem.*, 1990, **36**, 133.

(14) R. Akiyama, M. Kitaichi, T. Fujiwara, and S. Sawamura, *J. Nucl. Sci. Tech.*, 1994, **31**, 250.

(15) G.G. Jayson, B.J. Parsons, and A.J. Swallow, *J. Chem. Soc. Faraday Trans. 1, 1973, **69**, 1597.*

(16) V. Nagarajan and R.W. Fessenden, *J. Phys. Chem.*, 1985, **89**, 2330.

(17) P. Neta, R.E. Huie, and A.B. Ross, *J. Phys. Chem. Ref. Data*, 1988, **17**, 1027.

(18) W. Freyland, K. Garbade, and E. Pfeiffer, *Phys. Rev. Lett.* **1983,** *51*, 1304.

(19) D. Nattland, T. Rauch, and W. Freyland, *J. Chem. Phys.* **1993,** *98*, 4429.

(20) H.H. Kristoffersen and H. Metiu, *J. Phys. Chem. C* **2018,** *122*, 19603.

(21) S.J. Dai, *Raman Spectra*, 1995, **26**, 929.

(22) M. Kurley, *RSC Adv.*, 2019, **9**, 25602.

(23) J.F. Wishart, A.R. Cook, and J.R. Miller, *Rev. Sci. Instrum.* 2004, **75 (11)**, 4359.

(24) J.F. Wishart, J. Sun, M. Cho, C. Su, and S.S. Isied, *J. Phys. Chem. B*, 1997, **101**, 687.

(25) W.C. Phillips, R. Gakhar, G.P. Horne, B. Layne, K. Iwamatsu, A. Ramos-Ballesteros, M.R. Shaltry, J.A. LaVerne, S.M. Pimblott, J.F. Wishart, *Rev. Sci. Instrum.,* 2020, **91 (8)**, 083105.

(26) G.V. Buxton and C.R. Stuart, *J. Chem. Soc. Faraday Trans.*, 1995, **92**, 279.

(27) Pernot, P. SK-Ana: Analysis of Spectro-Kinetic Data (Version X.X), 2018, https://doi.org/10.5281/zenodo.1064370, last accessed on 03/14/2022.

(28) G.L. Hug, Optical Spectra of Nonmetallic Inorganic Transient Species in Aqueous Solution. U.S. Department of Commerce/National Bureau of Standards, NSRDS-NBS 69, *1981*.

(29) T.X. Wang, M.D. Kelley, J.N. Cooper, R.C. Beckwith, and D.W. Margerum, *Inorg. Chem.* 1994, **33**, 5872.

(30) M. Anbar and E.J. Hart, *J. Phys. Chem.*, 1965, **69**, 973.

(31) J.H. Baxendale, E.M. Fielden, and J.P. Keene, *Proc. Roy. Soc. (London) Ser. A*, 1965, **286**, 320.

(32) D. Meyerstein and W. A. Mulac, *Trans. Faraday Soc.*, 1969, **65**, 1818.

(33) F. Barat, L. Gilles, B. Hickel, and B. Lesigne, *J. Phys. Chem.* 1973, **77**, 1711.

(34) J. Rabani, W.A. Mulac, and M.S. Matheson, *J. Phys. Chem.*, 1977, **81**, 99.

(35) A. Blum and L.I.. Grossweiner *Photochem. Photobiol.* 1982, **36**, 617.

(36) R.K. Wolff, M. J. Bronskill and J. W. Hunt, *J. Chem. Phys.*, 1970, **53**, 4211.

(37) J.E. Aldrich, M.J. Bronskill, R.K. Wolff, and J.W. Hunt, *J. Chem. Phys.*, 1971, **55**, 530.

(38) K.Y. Lam and J.W. Hunt, *Int. J. Radiat. Phys. Chem.*, 1975, **7**, 317.

(39) C.D. Jonah, J.R. Miller, and M.S. Matheson, *J. Phys. Chem.*, 1977, **81**, 1618.

(40) J.F. Wishart, A.M. Funston, T. Szreder, A.R. Cook, and M. Gohdoa, *Faraday Discuss.*, 2012, **154**, 353.

(41) A.K. El Omar, U. Schmidhammer, B. Rousseau, J.A. LaVerne, and M. Mostafavi. *J. Phys. Chem. A*, 2012, **116 (47)**, 11509.

(42) G.V. Buxton and R.M. Sellers, *J. Chem. Soc., Faraday Trans. 1*, 1975, **71**, 558.

(43) G.V. Buxton, R.M. Sellers, D.R. McCracken, *J. Chem. Soc., Faraday Trans. 1*, 1976, **72**, 1464.

(44) I.E. Makarov, T.N. Zhukova, and A.K. Pikaev, *High Energy Chem.*, 1995, **29 (3)**, 151.

(45) C. Kwon, J. Kang, W. Kang, D. Kwak, and B. Han, *Electrochim. Acta* 2016, **195**, 216.

(46) G.J. Janz, F.W. Dampier, G.R. Lakshminarayanan, P.K. Lorenz, R.P.T. Tomkins, Molten Salts: Volume 1, Electrical Conductance, Density, and Viscosity Data, U.S. Department of Commerce/National Bureau of Standards, NSRDS-NBS61, Part II, 1979.

(47) V. K. Thorsmolle, G. Rothenberger, D. Topgaard, J. C. Brauer, D. B. Kuang, S. M. Zakeeruddin, B. Lindman, M. Gratzel and J. E. Moser, *ChemPhysChem*, 2011, **12**, 145.

(48) A. Byrne, E. M. Bringa, M. G. Del Popolo, J. J. Kohanoff, V. Galassi and N. J. English, *Int. J. Mol. Sci.*, 2019, **20**, 1123.